JOURNAL OF MATERIALS SCIENCE 33 (1998) 2735–2743

Densification of a rapidly solidified nickel aluminide powder-I application of hot-isostatic pressing diagrams

J. DUSZCZYK
Laboratory for Materials Science, Delft University of Technology, Rotterdamseweg 137, 2628 AL Delft, The Netherlands
E-mail: J. Duszczyk@stm.tudelft.nl

L. Z. ZHUANG,
Hoogoven Group, Research and Development, 1970 CA IJmuiden, The Netherlands

L. BUEKENHOUT
Boydcote Industrial Materials Technology, Industriepark-Noord 7, B-9100 Sint-Niklaas, Belgium

Densification of a gas-atomized, Cr-containing Ni_3Al-X intermetallic powder consolidated by hot isostatic pressing (HIP) was experimentally determined and also simulated using the Ashby model that describes mechanisms governing the deformation and consolidation during the process. The model has been applied to develop HIP diagrams, using best estimates or available values of input data on material properties so that the established HIP diagrams demonstrated a reasonable accuracy to allow prediction of the densification rates and controlling deformation mechanisms for this intermetallic alloy. It is believed that differences between the predicted and the experimentally determined densification of this material resulted mainly from the difficulty in estimating complex properties of this material which has an unusual property–temperature relationship and also from the deviation of the real particle size distribution from the monosized particle distribution used in the model.

1. Introduction

Consolidation of powders into monolithic forms using hot isostatic pressing (hip) is attractive because of the opportunity for near net shape production, especially for some materials which are difficult or expensive to produce by other means. The hipping process was initially developed as a means of diffusion bonding nuclear reactor components and for the removal of porosity in hard materials. However, the major commercial activity now centres upon the consolidation of metal powders and on the densification of high performance castings. Hipping involves the simultaneous application of a high pressure gas and an elevated temperature in a specially constructed vessel. The pressure applied is isostatic because it is developed with a gas. In general, therefore, no alteration in component geometry occurs. Under optimum conditions, encapsulated powder will be consolidated to give improved mechanical properties coupled with a reduced scatter band of properties as compared with those achieved through other processing routes. However, on the other hand, hipping is an expensive process. The optimum time–temperature–pressure combination, for achieving full density and providing high performance properties, is determined mainly by experiment. While the development of a programme to optimize a hipping schedule usually involves many runs. Therefore, considerable efforts have been made to model the hipping process which can predict densification rates and the dominant deformation mechanism for various combinations of time, temperature and pressure, and hence put the design of consolidation schedules on a more scientific basis [1–3].

During hipping, plastic flow, power law creep, Nabarro–Herring creep, Coble creep, grain boundary diffusion in the particles, and grain boundary and bulk diffusion at the particle contacts can all contribute to densification [4–7]. When a pressure is applied to packed powder particles, it is transmitted through the powder bed as a set of forces acting across the interparticle contact regions. The deformation at these contacts is at first elastic, but as the pressure rises, the contact forces increase, causing plastic yielding and expanding the points of contact into contact areas. Once these contact areas can support the forces without further yielding, time-dependent deformation processes will, therefore dominate the rate of further densification and form the basis of consolidation of powders during the hipping operation. However, which mechanism dominates the densification rate

depends also on a number of parameters related to the powder (particle size, grain size, geometry, mechanical, thermomechanical and physical properties) and to the processing (pressure, temperature and time).

Furthermore, the overall behaviour of densification during hipping is complicated because each densifying mechanism has a different dependence on particle size, on external variables, on powder properties and on the current effective pressure which is related to the current geometry [8]. In order to simplify the optimization process for hipping operations, hipping map construction by a computer programme has been developed by Ashby and co-workers [9, 10]. The hipping maps developed for individual alloy systems will be predictive when compared with experimental data. The computer programme is prepared mostly for the application to monolithic materials, although some models for the densification of composite powders have begun to appear in the literature [11, 12], based on models which predict densification rates and dominant densification mechanisms. Therefore, the constructed hipping maps can be practically used to identify the dominant mechanism and predict densification rates and times, as a function of pressure and temperature. They give guidance for the hipping operation to the most efficient combination of process variables. Application of hipping maps shows promise, although the construction of such maps requires knowledge of a variety of materials data which is sometimes very limited. It is also worthwhile emphasizing that the availability of a HIP diagram should permit optimization of temperature, pressure and time to achieve full density, while yet, prevent undue coarsening of the rapidly solidified microstructures, and permit control of the formation of desired phases.

It has been known that the intermetallic compound Ni_3Al exhibits increasing yield strength with increasing temperature up to about 700 °C, and has good resistance to oxidation. With the modification of this compound by boron and chromium additions, the problem of brittle failure at ambient temperatures and dynamic embrittlement at intermediate temperatures of the polycrystalline Ni_3Al has been largely overcome. On the other hand, although the addition of boron and chromium has resulted in modified alloys with substantial ductility, the nickel aluminides remain difficult to fabricate by conventional hot working methods. Therefore, processing these alloys by powder metallurgy techniques may be advantageous over the other processing routes. In addition, P/M processing can provide refined microstructures and largely suppress macrosegregation. However, the consolidation of this fine grained intermetallic with ordered lattice structure by plastic deformation was limited to the very beginning of the densification. Grain boundary and volume diffusion were also limited by the ordered structure. All these can influence the prediction of the densification behaviour of the powders using the existing models.

In this study, modeling of the hipping consolidation process has been performed and the constructed hipping maps have been used to investigate the densification behaviour of a nickel aluminide powder. A comparison between the experimental results and the predicted densification has been made to provide a basis for the development of future HIP cycles for Ni_3Al-based intermetallics. The influence of hipping variables on the microstructural development and mechanical properties of the consolidated material has also been studied and will be reported in Part II [13].

2. Material and experimental procedures

The material used in this study was a modified Ni_3Al-based intermetallic compound with alloying additions of boron, chromium and zirconium. The analysed chemical composition and impurities of the as-received powder are listed in Table I. The powder was provided by the GAPDRY plant of Höganäs AB, Sweden. The powder was prepared from a master ingot alloy which was induction melted under argon atmosphere and subsequently argon atomized. Particles larger than 250 μm were discarded by screening. The powder after sieving had a wide range in size distribution, as illustrated by the plot of cumulative weight against particle size and scanning electron microscopy (SEM) micrograph shown in Fig. 1, with a volume mean diameter d_{vm} of 75.7 μm. The SEM micrograph provides also a general view of the morphology of the powder particles which shows that the majority of the particles were spherical.

The powder was consolidated under a wide range of processing conditions. The material was first poured into commercial stainless steel tubes of 20 mm diameter, 2 mm thick, 600 mm long under argon gas protecting condition and sealed. The canned powder reached a packing (green) density of about 60–62% of the theoretical. After canning, the powder was consolidated by the hot isostatic pressing process at Boydcote Industrial Materials Technology Belgium. Most of the experiments were performed using a laboratory unit with a cylindrical sample chamber of 100 mm in diameter and 200 mm in height. Materials were also prepared for mechanical property investigations. In this case, a small production unit with a cylindrical chamber 250 mm diameter and 750 mm height was used. A total of 28 HIP runs were carried out to establish the influence of hipping conditions (temperature, pressure, and time) on the final density and

TABLE I Analysed chemical composition and impurity levels of the atomized powder (wt %)*

Al	Ni	Zr	Cr	B	Si	C	S	N	H	O
8.32	bal.	0.94	7.41	0.030	0.008	0.010	$\leqslant 0.005$	75	41	148

* p.p.m. for N, H, and O.

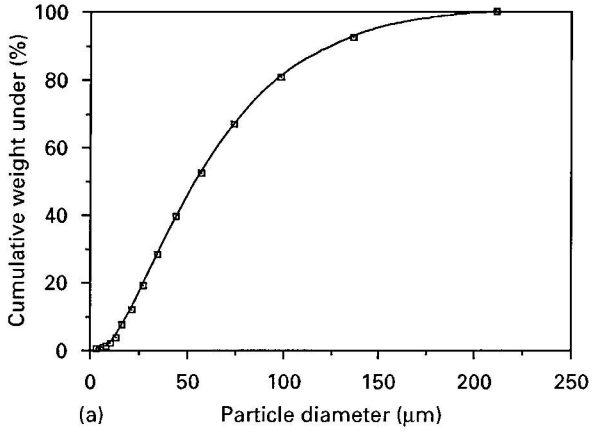

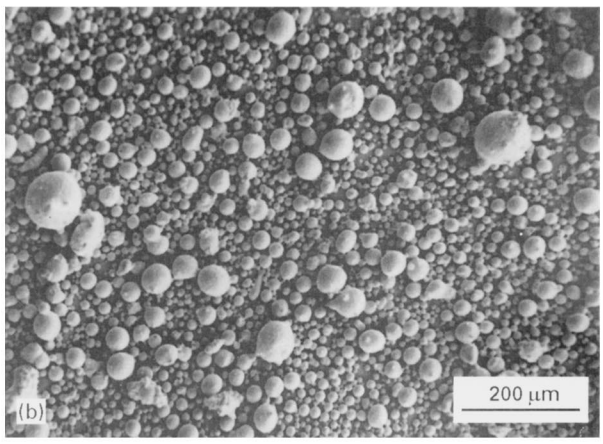

Figure 1 (a) size distributuion determined by the Malvern particle sizer and (b) SEM micrograph showing particle morphology of the intermetallic powder.

microstructure as well as mechanical properties. In general, the experiments can be divided into two series: one was at different temperatures of 850, 950, 1050, 1150, 1250 and 1330 °C, keeping the applied pressure constant at 100 MPa and a constant time of 30 or 120 min; and the other was at different pressures of 5, 10, 25, 50, 75, 100 and 150 MPa, holding the processing temperature constant at 950 or 1150 °C and a constant time of 30 or 120 min. A schematic drawing of typical temperature and load profiles used for hipping experiments is shown in Fig. 2.

Densities of the consolidated materials were determined by autopycnometry analysis in helium after evaporation of moisture at 150 °C for 5 min. Samples of about 20 g taken from the hipped bars were used for the measurements. Repeated measurements were made from several samples but prepared under the same hipping condition to assure accuracy. The samples were also checked by optical microscopy to confirm the measured results. The water immersion technique was also used to measure the densities of the consolidated samples which were in good agreement with those obtained by the autopycnometry analysis. The data presented in this discussion are from the autopycnometry analysis. Relative densities of the materials processed with different hipping parameters were calculated. On the other hand, a computer program developed by Ashby [9] has been used to construct hipping diagrams predicting the densification

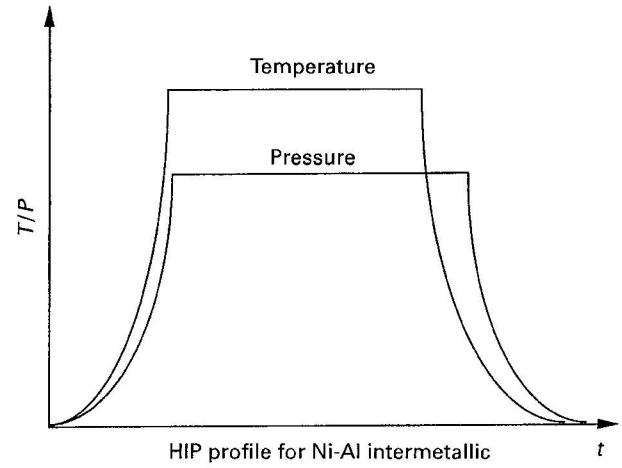

Figure 2 Typical temperature and pressure profile for a HIP cycle.

rates and the controlling deformation mechanisms for this intermetallic compound. The experimental results were compared with the calculated hipping maps.

3. Results and discussion

3.1. Experimental determination of the densification behaviour

Experimental results of the HIP consolidation on the Ni_3Al-based intermetallic powder are presented and discussed first, and then compared to the constructed hipping maps to identify the rate-controlling mechanisms.

The densification of the powder processed under various conditions is illustrated in Fig. 3. In all cases, the densities are given on a relative basis as a percentage of the theoretical density of the alloy. However, the density of the alloy is composition sensitive and no data were found in the literature for densities of modified Ni_3Al-based intermetallics except for the purely stoichiometric Ni_3Al which is reported with a density of 7.5 $Mg\,m^{-3}$ [14]. Therefore, in order to obtain the relative densities of the hipped materials, the theoretical density, ρ_{100}, for the alloy is calculated from:

$$\rho_{100} = \frac{4\overline{M}}{N_A V_C} \tag{1}$$

based on the results of chemical composition analysis and the lattice parameter obtained from the X-ray diffractometer measurement [15]. The number 4 represents 4 atoms in the unit cell of the f.c.c. structure, N_A is Avogadro's constant, $V_C = a_o^3$ is the unit cell volume, and $\overline{M}$ is the average atomic weight:

$$\overline{M} = \frac{\Sigma M_i \times \text{at}\%_i}{100} \tag{2}$$

The calculated theoretical density of the Cr-containing Ni_3Al-based alloy used in the present study is 7.726 $Mg\,m^{-3}$. It must be emphasized that the value calculated from Equation 1 is well consistent with that obtained by the autopycnometry measurements from

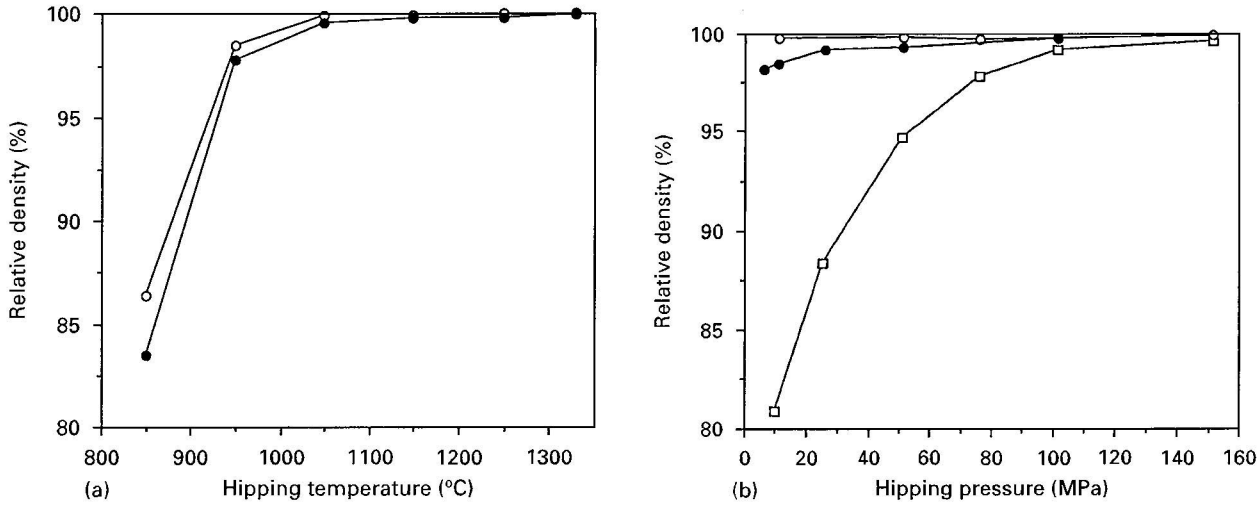

Figure 3 Experimental results showing the relationship between densification and process parameters (a) temperature for (○) 100 MPa/2 h and (●) 100 MPa/0.5 h and (b) pressure for (□) 950 °C/2 h, (○) 1150 °C/2 h and (●) 1150 °C/0.5 h.

the Osprey deposited and ingot materials after HIP treatment at temperatures higher than 1150 °C and a pressure of 100 MPa. According to a previous study [16] and microstructural examination of the HIP treated samples, it is believed that a full density of the Osprey deposited alloy can be achieved after the above HIP treatments. From the calculated theoretical density, ρ_{100}, and the measured densities, ρ_m, the relative densities of the hipped materials can be obtained.

It is seen in Fig. 3, that for the temperature and pressure intervals used in this work, the densification is much more responsive to the temperature change than to the pressure change. This is especially pronounced for the materials hipped at relatively lower temperatures, for example, at temperatures of 850 and 950 °C. The material hipped at 850 °C has a very low relative density, ~86%, while for the one hipped at 950 °C a reasonably high relative density, ~98.5%, is already achieved. Fig. 4 shows an optical micrograph of an unetched sample hipped at 850 °C. Most of the virtual porosity variation is a result of the two-dimensional sectioning of the packed spheres.

The results presented in Fig. 3 also indicate that the decreasing flow stress of the alloy particles with increasing temperature facilitates densification. In the present study, different pressures used during hipping at 1150 °C do not result in any significant influence on the relative density of the consolidated materials, a relative density of about 99.5% is already obtained even when a pressure of 10 MPa is applied. A high density is achieved at such a low pressure because the flow stress of the alloy at 1150 °C is very low. On the other hand, it should be realized that the effective stress, which is the stress at the interparticle contacts, is usually much higher than the external pressure applied during the initial stage of densification due to a low particle contact area related to a high porosity level. At the near-full density stage, further increase in density requires a higher applied pressure. This has been verified by the results obtained with varying pressure at 1150 °C.

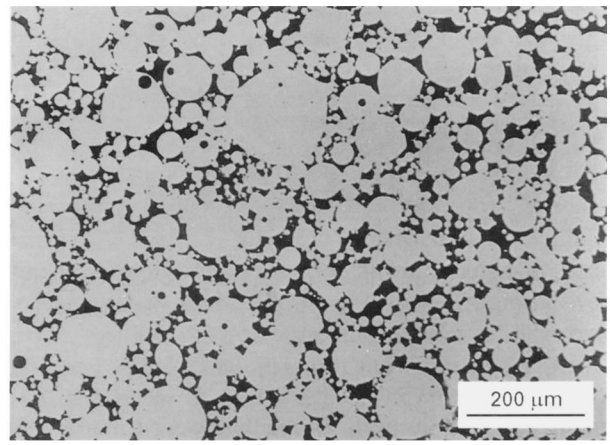

Figure 4 Optical micrograph showing the distribution of porosity in the material hipped at 850 °C.

3.2. Construction of hipping maps

The construction of hipping maps is based on rate equations for monolithic materials which describe the contributions from plastic flow, power law creep, volume and boundary diffusion, and Nabarro–Herring creep during consolidation of a monosize powder [8, 10]. It is assumed that densification is obtained at a rate that is the sum of individual contributions from several possible deformation mechanisms. Each densification mechanism is described by two sets of equations: one for the stage where a relative density is $< 90\%$ and pores are interconnected, and the other for higher relative densities with isolated pores. Basic equations used in this model are given as follows:

(1) stage I densification by plastic flow

$$D_i = \left\{ \frac{(1 - D_o)}{1.3\sigma_y} P + D_o^3 \right\}^{1/3} \tag{3a}$$

and stage II densification by plastic flow

$$D_i = 1 - \exp - \left[\frac{3P}{2\sigma_y} \right] \tag{3b}$$

(2) stage I densification rate by pressure driven volume diffusion

$$\dot{D} = 43C(1 - D_o)\frac{D_V}{r^2}\frac{(P - P_o)\Omega}{kT}S_1 \quad (4a)$$

and stage II densification rate by pressure driven volume diffusion

$$\dot{D} = 270(1 - D)^{1/2}\left[\frac{1 - D}{6}\right]^{1/3}\frac{D_V}{r^2}\frac{(P - P_i)\Omega}{kT}S_2 \quad (4b)$$

(3) stage I densification rate by surface tension driven volume diffusion

$$\dot{D} = 72CD_o\frac{D_V}{r^2}\frac{\gamma\Omega}{rkT}S_1 \quad (5a)$$

and stage II densification rate by surface tension driven volume diffusion

$$\dot{D} = 18\left[\frac{1 - D}{6}\right]^{1/3}\frac{D_V}{r^2}\left\{\frac{2\gamma}{r}\left[\frac{6}{1 - D}\right]^{1/3} - P_i\right\}\frac{\Omega}{kT}S_2 \quad (5b)$$

(4) stage I densification rate by pressure driven boundary diffusion

$$\dot{D} = 43C^2\frac{\delta D_B}{r^3}\frac{(P - P_o)\Omega}{kT}S_1 \quad (6a)$$

and stage II densification rate by pressure driven boundary diffusion

$$\dot{D} = 270(1 - D)^{1/2}\frac{\delta D_B}{r^3}\frac{(P - P_i)\Omega}{kT}S_2 \quad (6b)$$

(5) stage I densification rate by surface tension driven boundary diffusion

$$\dot{D} = 18\frac{CD}{(D - D_o)}\frac{\delta D_B}{r^3}\frac{\gamma\Omega}{rkT}S_1 \quad (7a)$$

and stage II densification rate by surface tension driven boundary diffusion

$$\dot{D} = 9\frac{\delta D_B}{r^3}\left\{\frac{2\gamma}{r}\left[\frac{6}{1 - D}\right]^{1/3} - P_i\right\}\frac{\Omega}{kT}S_2 \quad (7b)$$

(6) stage I densification rate by power law creep

$$\dot{D} = \frac{3.1}{C^{1/2}}D_{crp}D\left\{\frac{C(P - P_o)}{3\sigma_{ref}D^2}\right\}^n S_1 \quad (8a)$$

and stage II densification rate by power law creep

$$\dot{D} = 1.5D_{crp}D(1 - D) \times\left\{\frac{1.5}{n}\frac{(P - P_i)}{\sigma_{ref}}\frac{1}{1 - (1 - D)^{1/n}}\right\}^n S_2 \quad (8b)$$

(7) stage I densification rate by Nabarro–Herring, or diffusional creep

$$\dot{D} = 14.4\left\{\frac{D_V}{G^2} + \frac{\pi\delta D_B}{G^3}\right\}\frac{C^{1/2}}{D}\frac{(P - P_o)\Omega}{kT}S_1 \quad (9a)$$

and stage II densification rate by Nabarro–Herring, or diffusional creep

$$\dot{D} = 32\left\{\frac{D_V}{G^2} + \frac{\pi\delta D_B}{G^3}\right\}(1 - D)\frac{(P - P_1)\Omega}{kT}S_2 \quad (9b)$$

where

$$S_1 = 1 - \left(\frac{D - D_O}{0.95 - D_O}\right)^2 \quad \text{and} \quad S_1 = 0 \text{ if } D > 0.95$$

$$S_2 = 6.67D - 5.67 \quad \text{and} \quad S_2 = 0 \text{ if } D < 0.85$$

$$D_V = D_{OV}\exp^{-Q_V/RT}$$

$$\delta D_B = \delta D_{OB}\exp^{-Q_B/RT}$$

$$D_{crp} = 10^{-6}\exp - \frac{Q_{crp}}{RT_m}\left[\frac{T_m}{T} - 2\right]$$

$$C = \frac{1 - D_O}{D - D_O}$$

$$P_i = \left[\frac{1 - D_c}{1 - D}\right]\frac{D}{D_c}P_0$$

D	Relative density
D_O	Initial relative density (~ 0.62)
D_i	Relative density from plastic yielding
D_c	Relative density at which pores close (~ 0.95)
$\dot{D}$	dD/dt, densification rate (s^{-1})
δD_B	Boundary diffusion coefficient times its thickness ($m^3 s^{-1}$)
D_V	Volume diffusion coefficient ($m^2 s^{-1}$)
D_{OV}, D_{OB}	Pre-exponentials for volume and boundary diffusion ($m^2 s^{-1}$)
G	Grain size in particles (m)
k	Boltzmanns constant ($1.38 \times 10^{-23} JK^{-1}$)
n	Creep exponent
P	External pressure (MPa)
P_i	Internal pressure (MPa)
P_0	Outgassing pressure (MPa)
Q_B	Activation energy for boundary diffusion ($kJ mol^{-1}$)
Q_{crp}	Activation energy for creep ($kJ mol^{-1}$)
Q_V	Activation energy for volume diffusion ($kJ mol^{-1}$)
r	Particle radius (m)
R	Gas constant ($8.314 J mol^{-1} K^{-1}$)
γ	Surface tension ($J m^{-2}$)
S_1, S_2	Smoothing factors
T, T_m	Absolute temperature, absolute melting temperature (K)
t	Time (s)
σ	Stress (MPa)
σ_y	Yield stress (MPa)
σ_{ref}	Reference stress for creep (MPa)
Ω	Atomic volume (m^3)

The computer programme developed by Ashby sums up the densification rate contributions from each mechanism and integrates over time, with due consideration for a smooth transition between the two sets of equations for each mechanism, and gives the final relative density as a function of process variables and input parameters based on materials properties. Two types of diagrams can be constructed: i.e. the results can be plotted either as a function of temperature at constant pressure or as a function of pressure at constant temperature in the form of constant time contours. The constructed hipping maps also give the dominant fields for each mechanism.

The predictions are critically dependent on the material properties and other parameters used in the densification equations. The programme also includes an algorithm to approximate input values, when data are not available, from correlations established previously from a review of other published data [17, 18]. The values used in this study are presented in Table II [15, 19, 20]. The experimental hipping data were also referred for further refinement of the input parameters to obtain closer agreement with the predicted contours. In addition to the material properties, the powder particle size and grain size are also important inputs for the calculations.

The calculated maps presented in Figs 5 to 7 show five regions where specific mechanisms or stages dominate the densification rate. The hipping diagram in Fig. 5 shows the relative density of the Cr-containing Ni_3Al intermetallic powder consolidated at 100 MPa as a function of hipping temperature, while the map in Fig. 6 gives the relationship between the relative density and the hipping pressure at 1150 °C. Relative density of the powder consolidated at 950 °C is presented in Fig. 7, as a function of the hipping pressure.

TABLE II Input parameters for HIP maps

Material properties	Ni_3Al–Cr
Melting point, (K)	1663
Surface energy, ($J\,m^{-2}$)	1.0
Young's modulus, (GPa)	179
Temperature dependence of modulus	− 0.5
Yield strength, (MPa)	700
Temperature dependence of yield strength	− 1.0
Atomic volume, (m^3)	1.09×10^{-29}
Pre-exponent for volume diffusion, ($m^2\,s^{-1}$)	4.41×10^{-4}
Activation energy for volume diffusion, ($kJ\,mol^{-1}$)	306
Pre-exponent for boundary diffusion ($m^3\,s^{-1}$)	9.78×10^{-14}
Activation energy for boundary diffusion, ($kJ\,mol^{-1}$)	152
Pre-exponent for surface diffusion, ($m^3\,s^{-1}$)	1.00×10^{-10}
Activation energy for surface diffusion, ($kJ\,mol^{-1}$)	306
Power law creep exponent	3.0/4.5
Reference stress for power law creep, (MPa)	500/550
Activation energy for power law creep, ($kJ\,mol^{-1}$)	300
Solid density, ($kg\,m^{-3}$)	7726

3.3. Verification of calculated maps with experimental data

Densities determined experimentally are also incorporated in these maps for comparison. There exists, in general, a good agreement between the calculated diagrams and the experimental data. However, discrepancies arise at earlier stages of densification. For instance, at low temperatures the programme predicts a faster consolidation, while at high temperatures the programme predicts a lower consolidation rate. This resulted mainly from the difficulty in obtaining data on complex material properties which are required but are usually not available in the literature, especially the temperature dependence of yield strength and the modulus within the temperature region under consideration. There is also a certain deviation of the real particle size distribution from the monosized particle distribution used in the model.

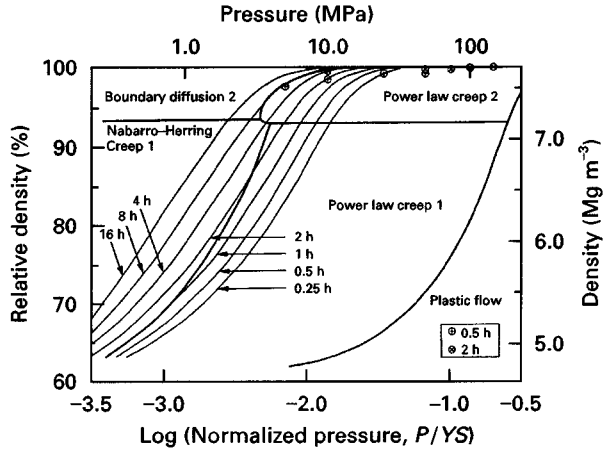

Figure 6 Calculated hipping map at a constant temperature of 1150°C superimposed with experimental data for the Ni_3Al-Cr intermetallic powder.

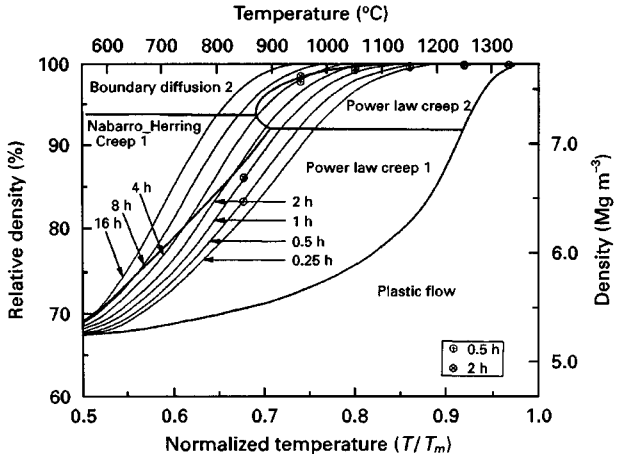

Figure 5 Calculated hipping map at a constant pressure of 100 MPa superimposed with experimental data for the Ni_3Al-Cr intermetallic powder.

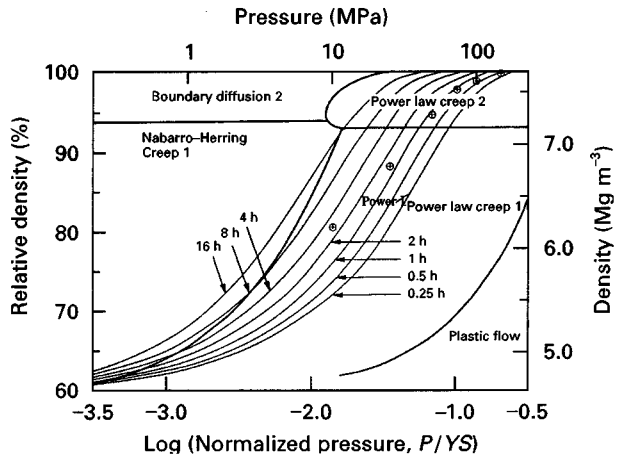

Figure 7 Calculated hipping map at a constant temperature of 950°C superimposed with experimental data for the Ni_3Al-Cr intermetallic powder.

The predicted hipping diagram Fig. 5 shows that at a constant pressure of 100 MPa power law creep is the dominant mechanism throughout the densification process when the processing temperature is higher than 1000 °C. At lower temperatures, the initial stage of the densification is dominated by power law creep and a combination of Nabarro–Herring creep and boundary diffusion becomes the primary mechanism for the later stages of densification. Both the experimentally determined and theoretically predicted results indicate that the final densification of the Ni_3Al-based intermetallic powder HIP consolidated within the temperature range between 950 and 1330 °C at 100 MPa, both for 0.5 h and 2 h, is dominated by the power law creep 2 (PLC-2) mechanism. Within this temperature range, variation in hipping temperature and time results in little change in the consolidated density. For the material hipped at 850 °C (100 MPa/2 h) the predicted contour shows a governing mechanism of the final densification being the Nabarro–Herring creep (N-HC) close to the boundary between the N-HC and PLC-1 dominant fields while the experimental result shows a location on the other side of the boundary within the PLC-1 dominant field. For the material hipped at 850 °C/100 MPa/0.5 h, a good agreement between the experimentally determined and theoretically predicted results is achieved, both are located in the PLC-1 dominant field. From these results, it is clear that the dominant mechanism for the densification of the 850 °C hipped material is different from that governing the final densification in the materials hipped at higher temperatures, a shift from the PLC-2 to the N-HC or the PLC-1 dominant field. As a result, a substantial difference in the relative densities between the materials consolidated at 850 and 950 °C is observed.

The calculated map, Fig. 6, shows that at 1150 °C the power law creep mechanism dominates the densification process for a wide range of the applied pressure. It is seen that only if the pressure is lower than, for instance 5 MPa, Nabarro–Herring creep and boundary diffusion mechanisms would become important for the later stages of the densification. The experimentally determined densities are, in general, higher than the predicted densification, especially for the materials hipped for 0.5 h. Due to the fact that a hipping temperature of 1150 °C is already rather high for this alloy, varying pressure within the range of 10 to 150 MPa and hipping time shows no significant effect on the relative density.

Fig. 7 shows the hipping map constructed at a temperature of 950 °C. As compared to Fig. 6, it is indicated that the densification time contours are shifted further to the power law creep regions with lower process temperature. At 950 °C, diffusion controlled mechanisms make little contribution to the total densification of the compacts. The material can be consolidated only when substantial deformation was achieved. Similar to the results obtained at 850 °C (Fig. 6), densities determined from experiments are in general lower than those estimated based on the Ashby model.

Discrepancies between the experimentally determined and theoretically predicted densification rates of the Ni_3Al-Cr intermetallic compound, as presented in Figs. 5 to 7, should be attributed to the uncertainty of some material properties with relation to the temperature. For instance, the temperature dependences of the modulus and the yield strength of the compound are assumed to have a positive response, in contrast to a negative response for many conventional materials, in the model within the whole range of temperatures considered. In practice, this is true only up to a certain temperature, and above that, the compound will also show a negative temperature dependence of these properties. However, the present model can not take this complex temperature dependence of properties into account. Therefore, as can be seen in Figs 5 and 6, the predicted densification rate at high temperatures is lower than the experimentally determined value due to the fact that a higher reference strength at high temperatures, based on the property-temperature dependence, is used in the model for calculation. This effect is less pronounced for the results obtained at low temperatures, as shown in Fig. 7 and in Fig. 5 for the material processed at 850 °C.

Optical micrographs presented in Fig. 8 illustrate the effect of temperature on the consolidation behaviour and microstructural development at a constant pressure and time, 100 MPa and 2 h. In agreement with the measured relative densities, the optical micrographs show a high porosity in the material hipped at 850 °C, a reasonably high density with small pores in the material hipped at 950 °C, and highly densified materials after hipping at higher temperatures. It is noted that at a hipping temperature of 850 °C, densification is dominated by establishing contact points between powder particles and the porosity is interconnected, as in Fig. 8a. At high temperatures, small pores are already isolated, as shown in Fig. 8b for 950 °C, and thereafter the individual pores shrink and disappear with increasing temperature, Fig. 8c to f. As indicated in Fig. 5, similar densification behaviour is observed for the samples processed for 0.5 h as for the samples hipped for 2 h.

Optical microscopy observation of other samples can be summarized as: (a) highly densified materials are obtained after hipping at 1150 °C with different pressures with no obvious difference in density between the samples processed for 2 h and 0.5 h, in agreement with that given in Fig. 6; (b) there is a clear relation between the density and hipping pressure for the samples processed at 950 °C as plotted in Fig. 7; (c) microstructures developed during the process are a function of processing temperature while processing pressure has little effect.

Based on the results obtained both from the relative density measurement and microstructure observation, it is apparent that full density can be achieved over a wide range of temperatures and pressures. However, our study [15] on the mechanical properties of the materials has proved that a higher temperature and pressure, for example 1250 °C and 100 MPa, has to be used for the hipping process in order to obtain the best properties. Hipping consolidation at a lower temperature or a lower pressure leads to a premature fracture of the material due to poor interparticle bonding SEM

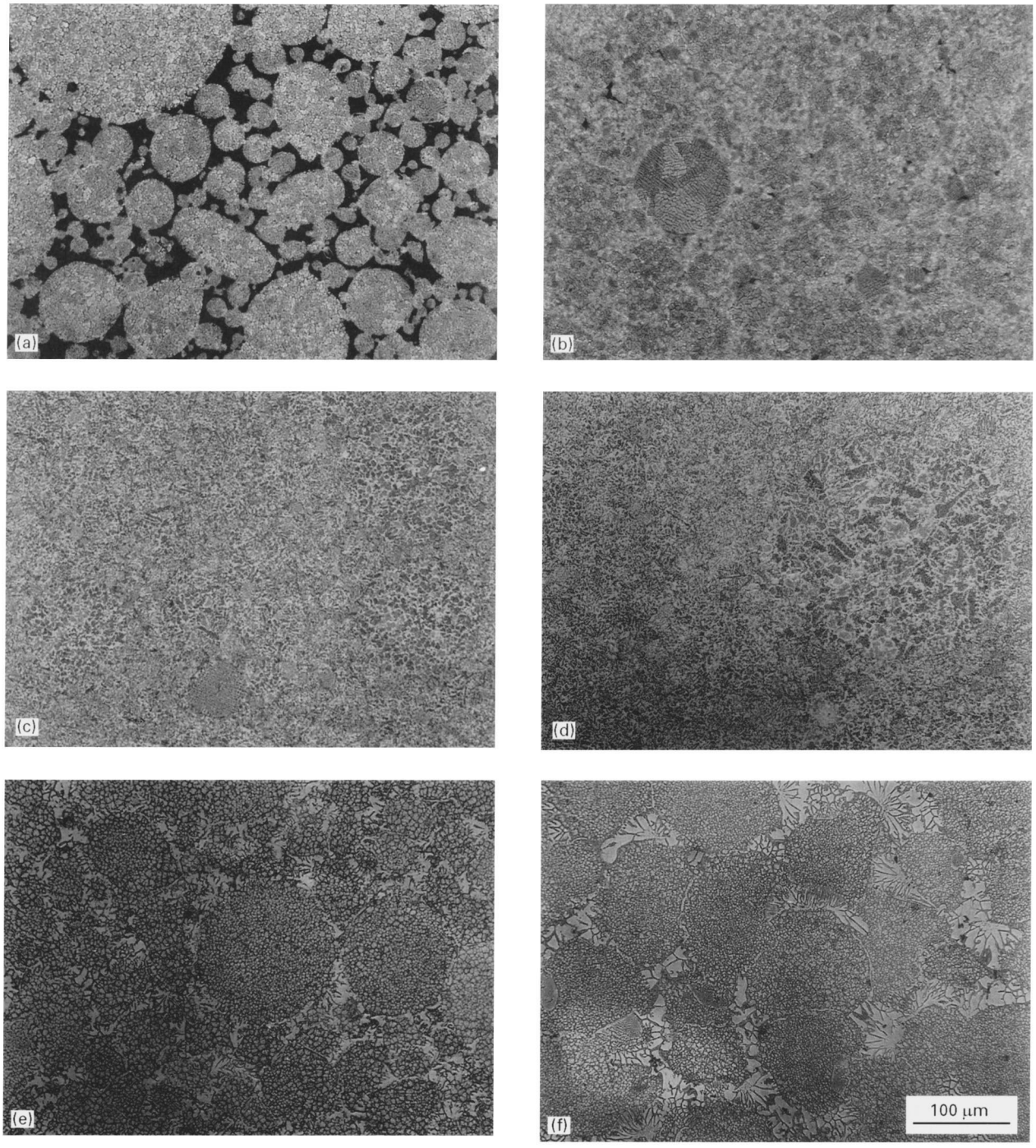

Figure 8 Optical micrographs showing the densification behaviour and microstructure evolution in the Ni_3Al-Cr intermetallic powder after hipping with 100 MPa for 2 h and at various temperatures of (a) 850 °C, (b) 950 °C, (c) 1050 °C, (d) 1150 °C, (e) 1250 °C and (f) 1330 °C.

examination of the fracture surfaces of the tensile samples shows a transition from interparticle fracture to transparticle fracture of the consolidated materials with increasing process temperature. Detailed discussion on the influence of hipping variables on the microstructural development and mechanical properties of the consolidated material will be reported in Part II.

4. Conclusions

The relationship between processing temperature and pressure and the final densification for the hipping process of the Ni_3Al-Cr intermetallic powder has been experimentally determined and the optimized processing parameters of 1250 °C/100 MPa/2 h have been established for this material. Based on available and estimated input data, hipping diagrams were constructed using the Ashby model to predict the densification rates and the dominant deformation mechanisms for this intermetallic compound. A good agreement between the constructed maps and experimental data is achieved. These results can be used as a basis for the development of future hipping cycles for the Ni_3Al-based intermetallics. However, a certain discrepancy between the experimental results and the predicted values has been observed under "extreme conditions". This may be attributed to the uncertainty of some material properties which have been used as input data for calculation with respect to temperature,

especially the temperature dependence of Young's modulus and yield strength. There is also a certain deviation of the real particle size distribution from the monosized particle distribution used in the model.

Acknowledgements

The authors are grateful for the assistance of Dr L. Kowalski in conducting the computer simulation experiments. The material was provided by the GAPDRY plant of Höganäs AB, Sweden. Hot isostatic pressing of the powder was performed by Boydcote Industrial Materials Technology Belgium.

References

1. M. F. ASHBY, in Proceedings of International Conference on "Hot isostatic pressing of materials: applications and developments", 25–27 April, 1988, Antwerp, Belgium. (The Royal Flemish Society of Engineers, (K. VIV), 1988) 1.1.
2. R. J. SCHAEFER, *Int. J. Powder Metall.* **28** (1992) 161.
3. M. M. CARROLL, *Metall. Trans. A* **17** (1986) 1977.
4. W. A. KAYSSER, M. ASLAN, E. ARZT, M. MITKOV and G. PETZOW, *Powder Metall.* **31** (1988) 63.
5. B. K. LOGRASSO and D. A. KOSS, *Metall. Trans. A* **19** (1988) 1767.
6. B. W. CHOI, Y. G. DENG, C. McCULLOUGH, B. PADEN and R. MEHRABIAN, *Acta Metall. Mater.* **38** (1990) 2225.
7. R. LAAG, W. A. KAYSSER, G. GALINSKI and R. MAURER, in Proceedings of International Conference on Powder Metallurgy "PM into the 1990's", 2–6 July, 1990, London, U.K., (The Institute of Metals, 1990) 278.
8. E. ARZT, M. F. ASHBY and K. E. EASTERLING, *Metall. Trans. A* **14** (1983) 211.
9. M. F. ASHBY, HIP 487: A program for constructing hot isostatic pressing diagrams, University of Cambridge, U.K. (1987).
10. A. S. HELLE, K. E. EASTERLING and M. F. ASHBY, *Acta Metall.* **33** (1985) 2163.
11. C. D. TURNER and M. F. ASHBY, in Proceedings of the International Conference on Hot Isostatic Pressing - HIP'93, 21–23 April, 1993, Antwerp, Belgium, edited by L. Delaey and H. Tas, (Elsevier Science B.V., 1994) 3.
12. R. M. McMEEKING, *Mech. Mater.* **12** (1991) 185.
13. J. DUSZCZYK, L. Z. ZHUANG and L. BUEKENHOUT, Part II of this contribution, submitted for publication.
14. K. VEDULA and J. R. STEPHENS, in Proceedings of Symposium on Powder Metallurgy 1986, edited by W. J. Huppmann, W. A. Kaysser and G. Petzow, (Verlag Schmid Gmbh, 1986) 205.
15. L. Z. ZHUANG, I. MAJEWSKA-GLABUS, R. VETTER, L. BUEKENHOUT and J. DUSZCZYK, in Proceedings of the Fourth International Conference on Isostatic Pressing, 5–7 November, 1990, Stratford-upon-Avon, U.K., (MPR Pbl. Shrewsbury, U.K., 1990) 21/1-24.
16. L. Z. ZHUANG, I. MAJEWSKA-GLABUS, R. VETTER, and J. DUSZCZYK, in Proceedings of the "P/M aerospace materials", November, 1991, Lausanne, Switzerland, (MPR Pbl., Shrewsbury, U.K., 1992) 9/1 - 18.
17. A. M. BROWN and M. F. ASHBY, *Acta Metall.* **28** (1980) 1085.
18. A. M. BROWN and M. F. ASHBY, *Scr. Metall.* **14** (1980) 1297.
19. R. N. WRIGHT, B. H. RABIN and J. R. KNIBLOE, *Mater. Manuf. Process.* **4** (1989) 25.
20. R. N. WRIGHT, R. L. WILLIAMSON and J. R. KNIBLOE, *Powder Metall.* **33** (1990) 253.

Received 9 September 1997
and accepted 13 February 1998